analytical chemistry

Article

Cite This: Anal. Chem. XXXX, XXX, XXX−XXX

pubs.acs.org/ac

Nitrosoreductase-Like Nanocatalyst for Ultrasensitive and Stable Biosensing

Ponnusamy Nandhakumar,[†] Byeongyoon Kim,[‡] Nam-Sihk Lee,[§] Young Ho Yoon,[§] Kwangyeol Lee,[‡] and Haesik Yang*[,†]

[†]Department of Chemistry and Chemistry Institute for Functional Materials, Pusan National University, Busan 46241, Korea

[‡]Department of Chemistry, Korea University, Seoul 02841, Korea

[§]EOne Laboratories, Incheon 22014, Korea

Supporting Information

ABSTRACT: Enzyme-like nanocatalytic reactions developed for high signal amplification in biosensors are of limited use because of their low reaction rates and/or unwanted side reactions in aqueous electrolyte solutions containing dissolved O_2. Herein, we report a nitrosoreductase-like catalytic reaction, employing 4-nitroso-1-naphthol, Pd nanoparticles, and $H_3N{-}BH_3$, which affords a high reaction rate and minimal side reactions, enabling its use in ultrasensitive electrochemical biosensors. 4-Nitroso-1-naphthol was chosen after five hydroxy-nitro(so)arene compounds were compared in terms of high signal and low background levels. Importantly, the nanocatalytic reaction occurs without the self-hydrolysis and induction period observed in the nanocatalytic reduction of nitroarenes by $NaBH_4$. The high signal level results from (i) fast nanocatalytic 4-nitroso-1-naphthol reduction, (ii) fast electrochemical redox cycling, and (iii) the low influence of dissolved O_2. The low background level results from (i) slow direct reaction between 4-nitroso-1-naphthol and $H_3N{-}BH_3$, (ii) slow electrode-mediated reaction between 4-nitroso-1-naphthol and $H_3N{-}BH_3$, and (iii) slow electrooxidation of $H_3N{-}BH_3$ at electrode. When applied to the detection of parathyroid hormone, the detection limit of the newly developed biosensor was ~0.3 pg/mL. The nitrosoreductase-like nanocatalytic reaction is highly promising for ultrasensitive and stable biosensing.

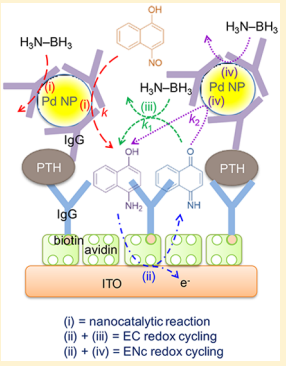

Nanocatalyst labels (or nanozyme labels) that allow rapid and high signal amplification, along with consistent and stable catalytic activity, have been extensively investigated in the development of ultrasensitive and highly reproducible biosensors.[1−4] The most common catalytic reactions employed in nanocatalyst labels, excluding electrocatalytic and photocatalytic processes, are (i) catalytic metal deposition on metal nanoparticles (NPs; e.g., Au NPs),[5] (ii) oxidase- or peroxidase-like oxidation of organic redox compounds by metal oxide NPs (e.g., cerium oxide and iron oxide NPs),[6,7] and (iii) nitroreductase-like reduction of organic nitroarene compounds by metal NPs (e.g., Au NPs).[8]

Catalytic metal deposition is widely used in biosensors and bioassays, particularly their colorimetric variants, because it is rapid and selective.[5,9] However, the catalytic oxidation of organic redox compounds has not been used in real biosensors because it is not as rapid and selective as the corresponding enzymatic reaction. Furthermore, the catalytic reduction of organic nitroarene compounds has not been used because rapid reduction requires an unstable strong reductant.[10,11] These limitations of catalytic oxidations and reductions of organic compounds mainly arise because they should be performed in aqueous electrolyte solutions containing dissolved O_2. Under these conditions, most strong reductants and oxidants are unstable and most catalytic redox reactions are slow or do not occur because a strong nucleophile (H_2O) and strong oxidant (O_2) are present. In many cases, electrolyte ions, especially Cl^-,[12] significantly decelerate catalytic redox reactions.

To obtain high electrochemical signal-to-background ratios in electrochemical biosensors, nanocatalyst substrates should be electroinactive over a given potential range, while nanocatalyst products should be highly electroactive. In this regard, the reduction of a hydroxy-nitroarene, such as 4-nitrophenol, to its corresponding hydroxy-aminoarene, such as 4-aminophenol, using nitroreductase-like nanocatalyst labels[8] is attractive because the electrochemical oxidation of hydroxy-aminoarenes readily occurs near 0 V versus Ag/AgCl, while the formal potential of a hydroxy-nitroarene is much higher than that of its corresponding hydroxy-aminoarene. A hydroxy-nitroarene contains a strong electron-withdrawing nitro group, while a hydroxy-aminoarene contains a strong electron-donating amine group. However, the catalytic nitroarene reduction requires an unstable strong reductant, such as $NaBH_4$, which undergoes self-hydrolysis in neutral and weak basic solutions and generates many bubbles.[13] Moreover, this catalytic reduction requires an induction period, perhaps due to the slow surface reconstruction of NPs[11] or the reduction of dissolved O_2 adjacent to NPs.[14] When milder strong reductants, such as

Received: August 19, 2017
Accepted: November 6, 2017

DOI: 10.1021/acs.analchem.7b03364
Anal. Chem. XXXX, XXX, XXX−XXX

hydrazine (H_2NNH_2), tris(2-carboxyethyl)phosphine (TCEP), and reduced β-nicotinamide adenine dinucleotide (NADH), are used, the catalytic nitroarene reduction is very slow or does not occur. Therefore, the practical application of catalytic nitroarene reduction to biosensors has been limited.

Six electrons are involved in the catalytic reduction of nitroarenes to aminoarenes, whereas four electrons are involved in the catalytic reduction of nitrosoarenes to aminoarenes.[15] Therefore, nitrosoarene reduction is easier to achieve than nitroarene reduction. However, the nanocatalytic reduction of nitrosoarenes has not been investigated and applied in biosensors, partly because nitrosoarene reduction by $NaBH_4$ occurs even in the absence of a nanocatalyst. Another strong reductant, ammonia–borane ($H_3N–BH_3$), which is a highly promising material for hydrogen storage, is very stable in air,[16,17] and dissolves readily and stably in aqueous solutions. The catalytic hydrolysis of $H_3N–BH_3$ using a metal nanocatalyst readily generates hydrogen[17] that can be used for the catalytic reduction of organic compounds. In recent years, $H_3N–BH_3$ has been applied to catalytic nitroarene reductions to evaluate the catalytic activities of nanomaterials.[18] To date, catalytic nitrosoarene reduction by $H_3N–BH_3$ has not been attempted in nanomaterials and biosensors.

When electrooxidation-based detection is performed in the presence of a strong reductant, an electrooxidized species can be reduced to the original signaling species and then reelectrooxidized. This electrochemical–chemical (EC) redox cycling[19,20] significantly increases electrochemical signals. Moreover, when a catalytic label is a redox enzyme or a redox nanocatalyst, label-mediated redox cycling can occur. These types of redox cycling are called electrochemical–enzymatic (EN) redox cycling[21,22] and electrochemical–nanocatalytic (ENc) redox cycling,[23] respectively, and both processes further increase the electrochemical signals. Therefore, when redox cycling is combined with a nanocatalytic reaction, very high signal amplification can be obtained.

Parathyroid hormone (PTH) is produced by the parathyroid glands and regulates blood calcium levels. The normal blood level of PTH is 10–65 pg/mL.[24,25] High or low PTH levels are related to bone diseases, hypocalcemia, and hypercalcemia. PTH detection is required for low and wide-ranging concentrations. Herein, we report a PTH biosensor that employs the catalytic reduction of nitrosoarenes by $H_3N–BH_3$ using Pd NPs [17 ± 4 nm, Figure S-1 in Supporting Information (SI)] as nanocatalysts (Figure 1a). Five hydroxy-nitro(so)arene compounds (Figure 1b) were tested and compared to obtain a high signal-to-background ratio. The combination of catalytic nitrosoarene reduction, EC redox cycling, ENc redox cycling, and low O_2 influence afforded high signal levels, and the combination of indium tin oxide (ITO) electrode, nitrosoarene, and $H_3N–BH_3$ afforded low background levels. The rate constants for EC and ENc redox cycling were measured to determine the relative contributions of EC and ENc redox cycling to the electrochemical signal. Finally, the new nanocatalytic reaction was applied to PTH detection (Figure 2a).

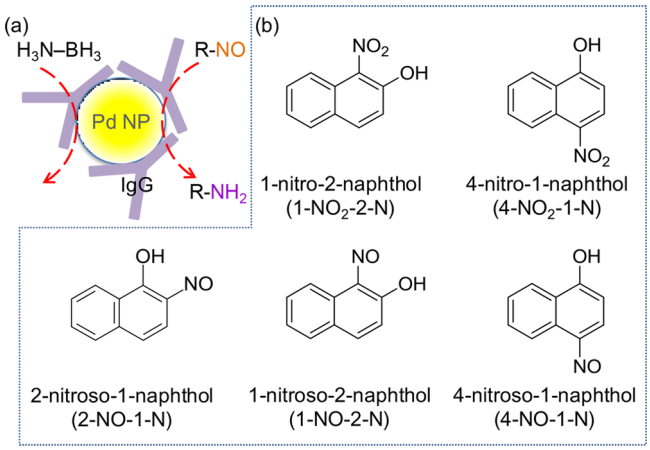

Figure 1. (a) Schematic diagram of catalytic reduction of a nitrosoarene using Pd nanoparticles (NPs). (b) Chemical structures of possible nanocatalyst substrates.

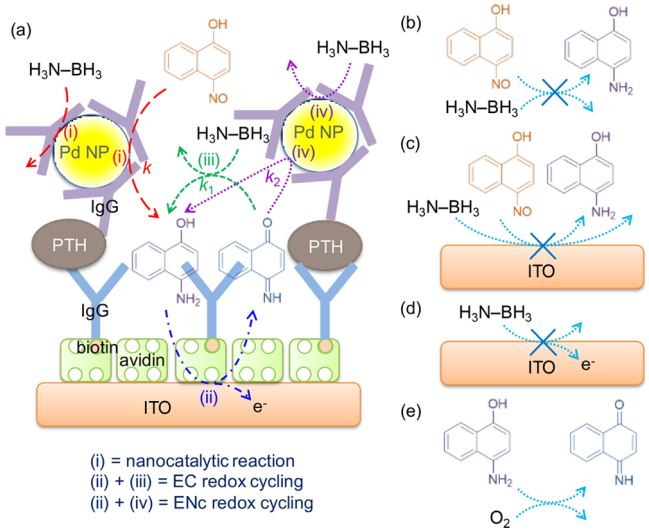

Figure 2. (a) Schematic diagram of an electrochemical immunosensor using Pd NPs as nanocatalytic labels. High signal amplification was obtained using (i) a nanocatalytic reaction, (ii + iii) electrochemical–chemical (EC) redox cycling, and (ii + iv) electrochemical–nanocatalytic (ENc) redox cycling. (b) Direct reaction of 4-nitroso-1-naphthol (4-NO-1-N) with $H_3N–BH_3$. (c) Indium tin oxide (ITO) electrode-mediated 4-NO-1-N reduction. (d) Direct electrooxidation of $H_3N–BH_3$ at an ITO electrode. (e) Nonelectrochemical oxidation of 4-amino-1-naphthol (4-NH_2-1-N) by O_2.

EXPERIMENTAL SECTION

Chemicals and Solutions. Avidin, 2-nitroso-1-naphthol (2-NO-1-N), 1-nitroso-2-naphthol (1-NO-2-N), 4-nitroso-1-naphthol (4-NO-1-N), 4-amino-1-naphthol (4-NH_2-1-N), $H_3N–BH_3$, H_2NNH_2, NADH, sodium cyanoborohydride ($NaBH_3CN$), ELISA blocking reagent (11112589001), citrate-stabilized Au NP (10 nm), and all reagents used for the preparation of buffer solutions were obtained from Sigma-Aldrich. 1-Nitro-2-naphthol (1-NO_2-2-N) and 4-nitro-1-naphthol (4-NO_2-1-N) were obtained from TCI. Human PTH protein (30R-2670), goat polyclonal anti-PTH IgG (70-XG67), and goat polyclonal anti-PTH IgG (70-XG68) were obtained from Fitzgerald, Inc. (Acton, MA, U.S.A.). Sulfosuccinimidyl-6-(biotinamido)-6-hexanamido hexanoate (EZ-link sulfo-NHS-LC-LC-biotin) was obtained from Thermo Fisher Scientific, Inc. (Meridian, Rockford, U.S.A.). Phosphate-buffered saline (PBS, pH 7.4) contained 10 mM phosphate, 0.138 M NaCl, and 2.7 mM KCl. PBSB (pH 7.4) contained all PBS ingredients and 1% (w/v) bovine serum albumin (BSA). PBSBT contained all PBSB ingredients and 0.05% Tween 20. Tris-buffered saline containing BSA (TBSB, pH 8.0) comprised 50 mM tris-

DOI: 10.1021/acs.analchem.7b03364
Anal. Chem. XXXX, XXX, XXX–XXX

(hydroxymethyl)aminomethane (tris), 0.138 M NaCl, 2.7 mM KCl, and 1% (w/v) BSA. Tris buffer (pH 9.0) for the electrochemical reaction contained 50 mM tris. Carbonate buffers (5 mM, pH 8.5; and 50 mM, pH 9.6) were prepared using sodium bicarbonate and sodium carbonate. All buffer and aqueous solutions were prepared using double-distilled water. ITO electrodes were obtained from Corning (Daegu, Korea). The synthetic procedures for Pd NPs and conjugation are provided in Supporting Information.

Preparation of Sensing Electrodes. ITO electrodes were pretreated with a 5:1:1 solution of H_2O, H_2O_2 (30%), and NH_4OH (30%), respectively, at 70 °C for 1 h. To obtain avidin-modified ITO electrodes, 70 μL of carbonate buffer (50 mM, pH 9.6) containing 10 μg/mL avidin was dropped onto the pretreated ITO electrodes. The avidin-dropped electrodes were maintained for 2 h at 20 °C. Subsequently, 70 μL of TBSB containing 0.1% ELISA blocking reagent was dropped onto the avidin-modified ITO electrodes, and the dropped state was maintained for 30 min at 4 °C. To immobilize biotinylated anti-PTH IgG, 70 μL of PBSB containing 10 μg/mL biotinylated anti-PTH IgG was dropped onto the avidin-modified ITO electrodes, and the dropped state was maintained for 30 min at 4 °C, followed by washing with PBSBT. The resulting electrodes were stored at 4 °C before use. To bind the target PTH to the immunosensing electrodes, 70 μL of PBSB (or human serum) containing different concentrations of PTH was dropped onto the immunosensing electrodes. This state was maintained for 30 min at 4 °C. Afterward, 70 μL of Pd NP-conjugated anti-PTH IgG (Pd NP−IgG conjugate) was dropped onto the target-treated electrodes, and this state was maintained for 30 min at 4 °C, followed by washing with PBSBT.

Electrochemical and Absorbance Measurements. Teflon electrochemical cells were assembled from the immunosensing electrode, a Ag/AgCl (3 M NaCl) reference electrode, and a Pt counter electrode. Tris buffer (1 mL) containing 2 mM $H_3N{-}BH_3$ and 0.2 mM 4-NO-1-N was injected into a vessel of the cell prior to measuring electrochemical signals. The exposed area of the immunosensing ITO electrode was approximately 0.28 cm^2. The final incubation was performed for 10 min at 25 °C and electrochemical measurements were carried out using a CHI 650E instrument (CH Instruments, Austin, TX, U.S.A.). PTH in the clinical serum samples was measured using the Cobas 8000 modular analyzer (Roche Diagnostics GmbH, Mannheim, Germany). The study protocol using clinical serum samples was approved by the Institutional Review Board of EOne Laboratories (#128477-201611-BR-011). UV−vis spectra were obtained using UV-1650 (SHIMADZU, Kyoto, Japan).

RESULTS AND DISCUSSION

Reactions that Influence the Signal-to-Background Ratio. For ultrasensitive detection, obtaining a high signal-to-background ratio is of utmost importance. In an electrochemical biosensor using a catalytic label, both chemical reactions and electrochemical reactions influence the signal-to-background ratio. Among various possible chemical reactions, a nanocatalytic reaction (reaction i in Figure 2a) that occurs in the presence of a nanocatalyst increases the signal level, whereas two unwanted reactions that occur in the absence of a nanocatalyst increase the background level. Unwanted reactions are direct reactions between the nanocatalyst substrate and a reductant (Figure 2b) and electrode-mediated reactions between the substrate and a reductant (Figure 2c), in which the electrode acts as a catalyst.

Among electrochemical reactions, the electrooxidation of a nanocatalyst product (reaction ii in Figure 2a) increases the signal level, whereas the direct electrooxidation of a reductant (Figure 2d) increases the background level. When electro-oxidation of a product (reaction ii in Figure 2a) is combined with the direct reaction of an oxidized form of a nanocatalyst product with a reductant (reaction iii in Figure 2a), EC redox cycling occurs, which further increases the signal level. When electro-oxidation of a product (reaction ii in Figure 2a) is combined with a nanocatalytic reaction of an oxidized form of a nanocatalyst product with a reductant (reaction iv in Figure 2a), ENc redox cycling occurs, which also further increases the signal level. However, the nonelectrochemical oxidation of a nanocatalyst product by dissolved O_2 (Figure 2e) decreases the apparent reaction rates of EC and ENc redox cycling, resulting in lower signal level. The influence of dissolved O_2 on a nanocatalytic reaction (reaction i in Figure 2a) also lowers the signal level.

Selection of Nanocatalyst Substrate. To select an appropriate nanocatalyst substrate that allowed a high signal-to-background ratio, two nitroarene compounds (1-NO_2-2-N and 4-NO_2-1-N) and three nitrosoarene compounds (2-NO-1-N, 1-NO-2-N, and 4-NO-1-N) (Figure 1b) were tested. In general, hydroxy-aminodiarene compounds have lower formal potentials and higher electrochemical reaction rates than their corresponding monoarene compounds.[26,27] The electrooxidation of hydroxy-aminodiarene compounds is rapid, even at bare ITO electrodes, whereas the fast electrooxidation of hydroxy-aminomonoarene compounds requires ITO electrodes modified with highly electrocatalytic materials.[28] Therefore, hydroxy-nitro(so)diarene compounds were chosen as potential substrates for catalytic conversion into readily electrooxidizable hydroxy-aminoarene compounds.

To investigate the signal and background levels resulting from only the nanocatalytic reaction (reaction i in Figure 2a), irrespective of electrode-mediated catalytic reactions (Figure 2c), time-course absorbance data were obtained in a glass cuvette filled with a solution containing a nanocatalyst substrate and reductant (Figure 3 and SI, Figure S-2). Among four reductants (H_2NNH_2, $NaBH_3CN$, NADH, and $H_3N{-}BH_3$), only $H_3N{-}BH_3$ reduced 4-NO-1-N catalytically in the presence of Pd NPs (SI, Figure S-2). Therefore, $H_3N{-}BH_3$ was selected as the reductant for the catalytic reduction of nitro(so)arene compounds. In the absence of Pd NPs, the absorbance in a solution containing a nanocatalyst substrate and $H_3N{-}BH_3$ did not change with time in all five cases (Figure 3a), indicating that a direct reaction between each substrate and $H_3N{-}BH_3$ (Figure 2b) was very slow or did not occur. However, nitrosoarene compounds were readily reduced by $NaBH_4$ and TCEP in the absence of catalyst (data not shown).

In the presence of Pd NP−IgG conjugates, the absorbance decreased with time in all cases (Figure 3b). This result clearly showed that both nitroarenes and nitrosoarenes could be catalytically reduced. Importantly, the absorbance decreased without the induction period observed when nitroarenes are catalytically reduced by $NaBH_4$.[11,14] The reduction of nitrosoarenes (curves viii, ix, and x in Figure 3b) was faster than that of nitroarenes (curves vi and vii in Figure 3b). These results showed that $H_3N{-}BH_3$ was a good reductant that allowed a high signal-to-background ratio for all five potential substrates when only considering the nanocatalytic reaction. Although

DOI: 10.1021/acs.analchem.7b03364
Anal. Chem. XXXX, XXX, XXX−XXX

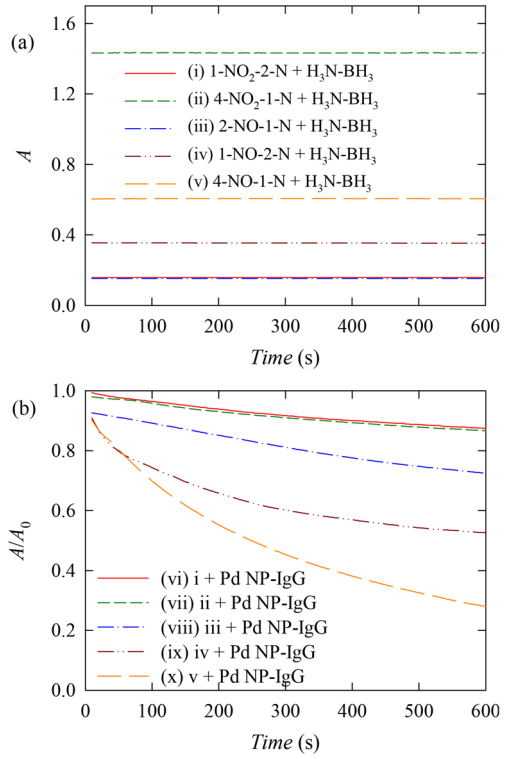

Figure 3. (a) Time-course data of absorbance (A) at 25 °C in tris buffer (pH 9.0) containing 2.0 mM $H_3N{-}BH_3$ and 50 μM of (i) 1-NO_2-2-N, (ii) 4-NO_2-1-N, (iii) 2-NO-1-N, (iv) 1-NO-2-N, or (v) 4-NO-1-N. (b) Time-course data of A/[initial absorbance (A_0)] at 25 °C in tris buffer (pH 9.0) containing 2.0 mM $H_3N{-}BH_3$, 5−10 μg/mL Pd NP−IgG conjugate and 50 μM of (vi) 1-NO_2-2-N, (vii) 4-NO_2-1-N, (viii) 2-NO-1-N, (ix) 1-NO-2-N, and (x) 4-NO-1-N. The absorbance was measured at the wavelength of maximum absorbance: (i, vi) 436, (ii, vii) 458, (iii, viii) 431, (iv, ix) 379, and (v, x) 404 nm.

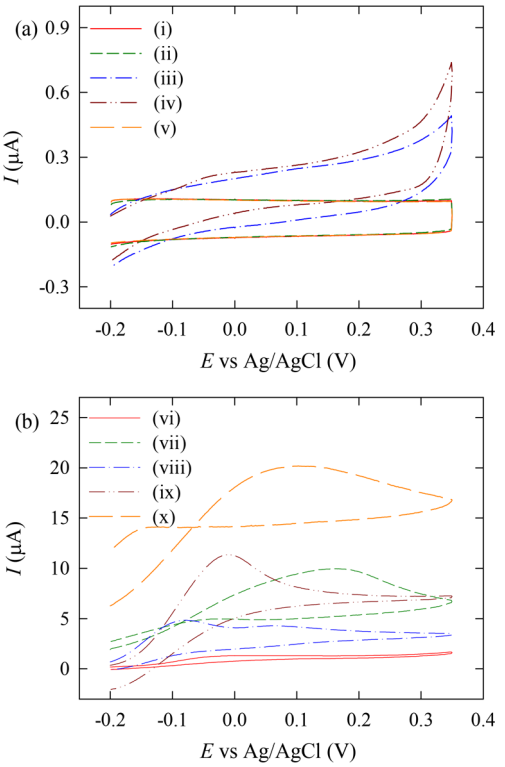

Figure 4. Cyclic voltammograms obtained at ITO electrodes at a scan rate of 20 mV/s after an incubation period of 10 min at 25 °C in (a) tris buffer (pH 9.0) containing 2.0 mM $H_3N{-}BH_3$ and 0.2 mM of (i) 1-NO_2-2-N, (ii) 4-NO_2-1-N, (iii) 2-NO-1-N, (iv) 1-NO-2-N, and (v) 4-NO-1-N; and (b) tris buffer (pH 9.0) containing 2.0 mM $H_3N{-}BH_3$, 1 μg/mL Pd NP, and 0.2 mM of (vi) 1-NO_2-2-N, (vii) 4-NO_2-1-N, (viii) 2-NO-1-N, (ix) 1-NO-2-N, and (x) 4-NO-1-N.

$H_3N{-}BH_3$ did not reduce nitro(so)arenes directly, it did reduce them catalytically in the presence of Pd NP−IgG conjugates.

The time course data for catalytic 4-NO-1-N reduction were fitted with eq 1 by assuming the pseudo-first order reaction (SI, Figure S-3).[14]

$$C/C_0 = \exp(-k_{app}t) = \exp(-kSt) \quad (1)$$

where C is the concentration of 4-NO-1-N at time t, C_0 is its initial concentration, k_{app} is the apparent rate constant, and k is the rate constant normalized to the nanoparticle surface area S (m^2/L). The calculated k_{app} and k for Pd NP−IgG conjugate were 2.88×10^{-3} s^{-1} and 0.20 $s^{-1}L/m^2$, respectively. The k for unconjugated Pd NP was 1.12 $s^{-1}L/m^2$. It indicates that the IgG on Pd NP decreased the rate of catalytic reduction 5.5×. Importantly, these k values are comparable to the values for catalytic 4-nitrophenol reduction by $NaBH_4$ in the presence of Pd NP.[14]

To investigate the signal and background levels resulting from all chemical and electrochemical reactions, cyclic voltammograms were measured after an incubation period of 10 min in a solution containing a nanocatalyst substrate and $H_3N{-}BH_3$ in contact with an ITO electrode (Figure 4). Interestingly, for 2-NO-1-N and 1-NO-2-N (ortho-substituted nitrosoarenes) the anodic currents observed in the cyclic voltammograms were higher than the capacitive background currents, even in the absence of Pd NPs (Figure 4a). Considering that the direct reaction of ortho-substituted nitrosoarenes with $H_3N{-}BH_3$ did not occur or was very slow, as shown in Figure 3a, this result indicated that an ITO electrode-mediated reaction occurred between ortho-substituted nitrosoarenes and $H_3N{-}BH_3$ (Figure 2c). Although the ITO electrode-mediated reaction of ortho-substituted nitrosoarenes was slower than the catalytic reduction obtained in the presence of Pd NPs, it increased the background level significantly. For 1-NO_2-2-N, 4-NO_2-1-N, and 4-NO-1-N (two nitroarenes and a para-substituted nitrosoarene), the anodic currents were similar to the capacitive background currents (Figure 4a), indicating that the ITO electrode-mediated reaction did not occur or was very slow.

In the presence of Pd NPs, the observed anodic currents were much higher than the capacitive background currents in all cases (Figure 4b). The current levels were much higher than those obtained in the absence of Pd NPs (Figure 4a). These higher current levels confirmed that all five nitro(so)arenes could be reduced catalytically by $H_3N{-}BH_3$ in the presence of Pd NPs, as demonstrated by the absorbance data in Figure 3b. The high current levels resulted from fast EC redox cycling (reactions ii and iii in Figure 2a) and fast ENc redox cycling (reactions ii and iv in Figure 2a), along with the fast nanocatalytic reduction. The anodic currents for 4-NO-1-N (curve x in Figure 4b) were much higher than those of the other substrates. Because of the nonelectrochemical oxidation of 4-NH_2-1-N by dissolved O_2 (Figure 2e), EC and ENc redox cycling were influenced by dissolved O_2. Moreover, nanocatalytic nitro(so)arene reduction was also influenced by

DOI: 10.1021/acs.analchem.7b03364
Anal. Chem. XXXX, XXX, XXX−XXX

dissolved O_2. However, the influence of dissolved O_2 in an air-saturated solution was not high enough to decrease the electrochemical signals significantly (SI, Figure S-4). Compared to tris buffer (pH 9.0), the catalytic reduction of 4-NO-1-N in acetate buffer (pH 4.0) and PBS (pH 7.4) was much slower (SI, Figure S-5). It is because the higher pH was better for nanocatalytic nitrosoarene reduction.

To compare the signal-to-background ratios quantitatively, chronocoulograms were measured for all five nitro(so)arenes at bare ITO electrodes and ITO electrodes modified with adsorbed Pd NP−IgG conjugates (SI, Figure S-6). The charge values of chronocoulograms obtained in the absence of Pd NPs correspond to the background levels, whereas the charge values obtained at the modified electrodes correspond to the signal levels. Substrates 1-NO_2-2-N, 4-NO_2-1-N, and 4-NO-1-N gave the lowest background levels (SI, Figure S-6a), while 4-NO-1-N gave the highest signal level (SI, Figure S-6b). Figure 5 shows a

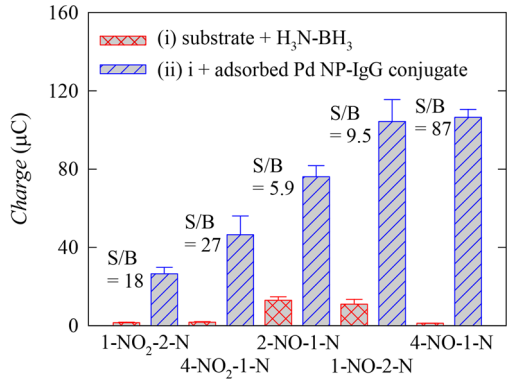

Figure 5. Histogram of signal-to-background ratios calculated from the charge values measured at 100 s with chronocoulograms (SI, Figure S-6) obtained at an applied potential of 0.10 V at (i) bare ITO electrodes and (ii) ITO electrodes modified with adsorbed Pd NP−IgG conjugate after an incubation period of 10 min at 25 °C in tris buffer (pH 9.0) containing 0.2 mM substrate and 2.0 mM H_3N−BH_3.

histogram of the signal-to-background ratios for the five nitro(so)arenes. Nitrosoarenes performed better than nitroarenes, while para-substituted nitrosoarenes performed better than their ortho-substituted counterparts. 4-NO-1-N obtained the highest signal-to-background ratio. Optimal concentrations of 4-NO-1-N and H_3N−BH_3 were 0.2 and 2.0 mM, respectively (SI, Figure S-7).

In biosensors, Au NPs are more widely employed as labels than Pd NPs. When Au NPs (10 nm) were used for nanocatalytic reduction of 4-NO-1-N by H_3N−BH_3, the observed anodic currents (SI, Figure S-8) were smaller at low potentials than the anodic currents for Pd NPs (curve x in Figure 4b). For comparison between Au NPs and Pd NPs, the concentration of Au NPs was adjusted to ensure that the total surface area of Au NPs was the same as that of Pd NPs. The result showed that Pd NPs was better for obtaining a high signal level than Au NPs.

Consequently, a high signal level was obtained from (i) fast catalytic 4-NO-1-N reduction; (ii) fast EC redox cycling involving the ITO electrode, 4-NH_2-1-N, and H_3N−BH_3; (iii) fast ENc redox cycling involving the ITO electrode, 4-NH_2-1-N, Pd NPs, and H_3N−BH_3; and (iv) the low influence of dissolved O_2 on these reactions (Figure 2). A low background level was obtained from (i) the slow direct reaction of 4-NO-1-N with H_3N−BH_3, (ii) the slow ITO-mediated reaction between 4-NO-1-N and H_3N−BH_3, and (iii) the slow electrooxidation of H_3N−BH_3 at the ITO electrode (Figure 2).

Rate Constants for EC and ENc Redox Cycling. Both EC and ENc redox cycling contributed to the electrochemical signal, as shown in Figure 2a. To determine the relative contribution of EC and ENc redox cycling to the electrochemical signals, the rate constants for EC and ENc redox cycling (k_1 and k_2 in Figure 2a) were measured from chronoamperograms, as shown in Figure 6. The limiting

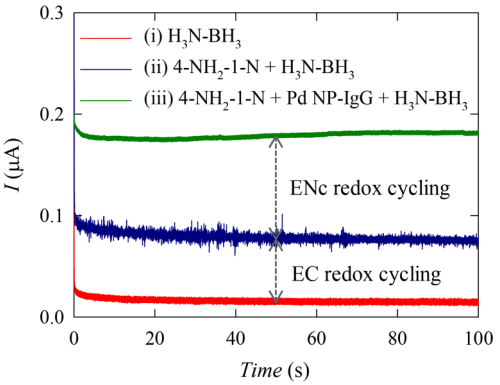

Figure 6. Chronoamperograms obtained at 0.35 V at avidin- and BSA-modified ITO electrodes at 25 °C in tris buffer (pH 9.0) containing (i) 5.0 mM H_3N−BH_3, (ii) 0.05 mM 4-NH_2-1-N and 5.0 mM H_3N−BH_3, and (iii) 0.05 mM 4-NH_2-1-N, 1 μg/mL−10 μg/mL Pd NP−IgG conjugate, and 5.0 mM H_3N−BH_3.

currents at 50 s in the chronoamperograms were used to calculate the rate constants. When the concentration of H_3N−BH_3 (5.0 mM) was 100× higher than that of 4-NH_2-1-N (0.05 mM) and the applied potential in chronoamperometry (0.35 V) was much higher than the formal potential of 4-NH_2-1-N, the rate constant of EC redox cycling (k_1 in Figure 2a) could be calculated from the difference (I_{EC}, 6.76×10^{-8} A) between the limiting current obtained in the presence of 4-NH_2-1-N and H_3N−BH_3 and the limiting current obtained in the presence of H_3N−BH_3 alone.[20,29]

$$I_{EC} = nFAC_{4\text{-NH2-1-N}}\sqrt{D_{4\text{-NH2-1-N}}k_1C_{H3N\text{-}BH3}} \quad (2)$$

where $C_{4\text{-NH2-1-N}}$ and $C_{H3N-BH3}$ are the concentrations of 4-NH_2-1-N and H_3N−BH_3, respectively, $D_{4\text{-NH2-1-N}}$ is the diffusion coefficient of 4-NH_2-1-N (6.3×10^{-6} cm^2/s),[30] n is the number of electrons involved (it was assumed that two electrons were involved), and F and A are the Faradaic constant and electrode area (0.28 cm^2), respectively. The rate constant of ENc redox cycling (k_2 in Figure 2a) was calculated from the difference (I_{ENc}, 9.84×10^{-8} A) between the limiting current obtained in the presence of 4-NH_2-1-N, Pd NP−IgG conjugate, and H_3N−BH_3, and the limiting current obtained in the presence of 4-NH_2-1-N and H_3N−BH_3.[31,32]

$$I_{ENc} = nFAC_{4\text{-NH2-1-N}}\sqrt{D_{4\text{-NH2-1-N}}k_2C_{Pd\,NP}} \quad (3)$$

where $C_{Pd\,NP}$ is the concentration of Pd NP in Pd NP−IgG conjugate (54 pM).

The calculated apparent rate constants k_1 and k_2 were 2.0×10^{-2} and 3.9×10^6 M^{-1} s^{-1}, respectively. Because of the nonelectrochemical oxidation of 4-NH_2-1-N by dissolved O_2 (Figure 2e), the real k_1 and k_2 would be higher than the apparent k_1 and k_2 measured in air-saturated solutions containing dissolved O_2. The apparent k_1 for EC redox cycling

DOI: 10.1021/acs.analchem.7b03364
Anal. Chem. XXXX, XXX, XXX−XXX

was lower than the rate constant for EC redox cycling of 4-aminophenol by H_2NNH_2 ($7.1 \times 10\ M^{-1}\ s^{-1}$).[20] The apparent k_2 for ENc redox cycling was comparable with the apparent rate constant for EN redox cycling using DT-diaphorase ($3.3 \times 10^6\ M^{-1}\ s^{-1}$).[22] Although the apparent k_1 for EC redox cycling was much smaller than the apparent k_2 for ENc redox cycling, the contribution of EC redox cycling to the total current was considerable because the $H_3N{-}BH_3$ concentration was much larger than that of the Pd NP labels, which were affinity-bound to the immunosensing electrode. The high apparent k_2 for ENc redox cycling allowed high signal amplification, even when the concentration of the Pd NP labels on the immunosensing electrode was very low.

PTH Detection. To obtain a low detection limit in the immunosensor shown in Figure 2a, it was important to minimize the nonspecific binding of the Pd NP−IgG conjugate. When Pd NP−IgG conjugate was present in carbonate buffer (pH 8.5) containing BSA, the nonspecific binding was lower than that in carbonate buffer (SI, Figure S-9). A concentration of 0.1% BSA was optimal for low nonspecific binding of Pd NP−IgG conjugate (SI, Figure S-9). As the concentration of Pd NP−IgG conjugate used during detection process was increased, electrochemical signal level was increased but background level due to nonspecific binding was also increased. When the concentration of Pd NP was increased during the preparation of Pd NP−IgG conjugate, low nonspecific binding was maintained up to 5 μg/mL Pd NP (SI, Figure S-10). Therefore, the Pd NP−IgG conjugate prepared with this concentration was used for immunosensing.

The immunosensing scheme in Figure 2a was applied to PTH detection. PTH in the sample was captured by IgG on an immunosensing electrode, and Pd NP−IgG conjugate was then bound to the captured PTH. Pd NPs converted 4-NO-1-N into 4-NH_2-1-N over an incubation period (reaction i in Figure 2a). When 4-NH_2-1-N was electrochemically oxidized, EC redox cycling (reactions ii and iii in Figure 2a) and ENc redox cycling (reactions iv and v in Figure 2a) were induced. The combination of the nanocatalytic reaction, EC redox cycling, and ENc redox cycling afforded a high signal level, and the combination of the ITO electrode, 4-NO-1-N, and $H_3N{-}BH_3$ afforded a low background level.

To obtain concentration-dependent data, chronocoulograms were measured after the immunosensing electrodes were treated with various concentrations of PTH in PBSB (Figure 7a). The charge slope increased with increasing PTH concentration. The charge values measured at 100 s were used to obtain a calibration curve in Figure 7b, which showed that PTH could be detected over a wide concentration range. The calculated detection limit for PTH were ~0.3 pg/mL.

To further evaluate the new immunosensor, the PTH concentration in clinical serum samples was measured and the results compared with measurements performed using a commercial instrument. The PTH concentrations calculated using the calibration curve in Figure 7b were in good agreement with the actual PTH concentrations (Figure 7c). These results indicated that the new nanocatalytic reaction was promising for use in ultrasensitive and stable biosensors and bioassays.

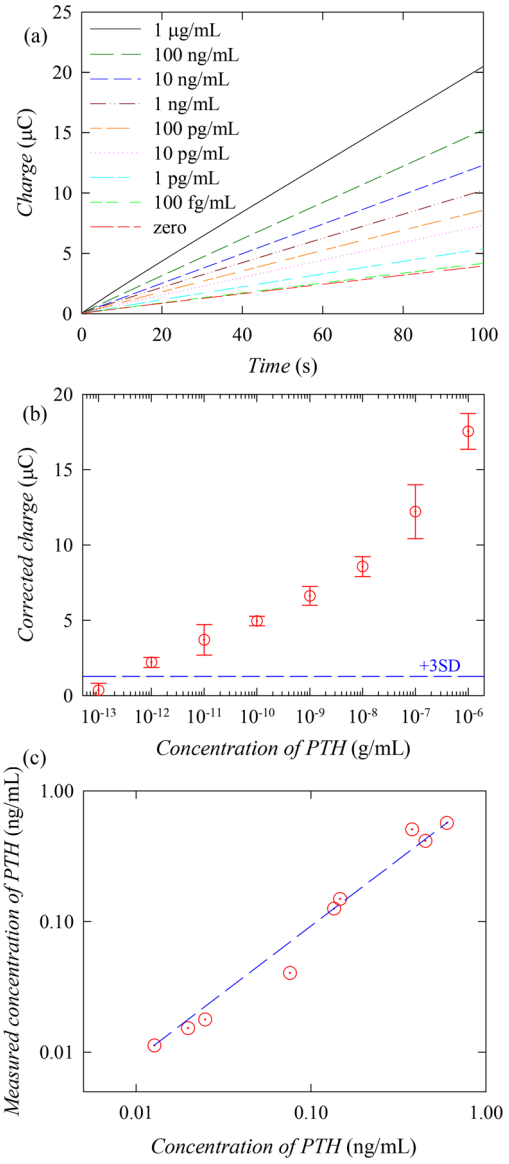

Figure 7. (a) Chronocoulograms obtained at an applied potential of 0.10 V using immunosensing electrodes and various PTH concentrations in PBSB after an incubation period of 10 min at 25 °C in tris buffer (pH 9.0) containing 0.2 mM 4-NO-1-N and 2.0 mM $H_3N{-}BH_3$. (b) Calibration curve for the charge values measured at 100 s from the chronocoulograms in panel a. All experiments were conducted using three different electrodes for each sample. All data were subtracted from the mean value at zero concentration, determined from seven measurements. Dashed line corresponds to three times the standard deviation (SD) of the charge value at zero concentration. Error bars represent the SD of three measurements. (c) Comparison of the concentration of PTH measured with the immunosensor (the average value of three measurements) and the concentration of PTH measured with a commercial instrument for nine actual clinical serum samples.

CONCLUSIONS

We have developed a nitrosoreductase-like nanocatalytic reaction employing 4-NO-1-N, Pd NP and $H_3N{-}BH_3$ and applied the reaction to a practically appealing electrochemical biosensor. Importantly, the catalytic reaction was performed without two critical problems (the self-hydrolysis and induction period) that are commonly observed in nanocatalytic nitroarene reduction by $NaBH_4$. The high signal level results from (i) fast catalytic 4-NO-1-N reduction, (ii) fast EC redox cycling involving ITO electrode, 4-NH_2-1-N and $H_3N{-}BH_3$, (iii) fast ENc redox cycling involving ITO electrode, 4-NH_2-1-N, Pd NP, and $H_3N{-}BH_3$, and (iv) the low influence of dissolved O_2. The low background level results from (i) slow direct reaction

DOI: 10.1021/acs.analchem.7b03364
Anal. Chem. XXXX, XXX, XXX−XXX

between 4-NO-1-N and H_3N-BH_3, (ii) slow ITO-mediated reaction between 4-NO-1-N and H_3N-BH_3, and (iii) slow electrooxidation of H_3N-BH_3 at ITO electrode. When the newly developed biosensor was applied to the detection of parathyroid hormone, the detection limit was ~0.3 pg/mL in PBSB. The nitrosoreductase-like nanocatalytic reaction is highly promising for ultrasensitive and stable biosensing.

■ ASSOCIATED CONTENT

Supporting Information

The Supporting Information is available free of charge on the ACS Publications website at DOI: 10.1021/acs.analchem.7b03364.

Procedures for Pd NP synthesis and conjugation, TEM image of Pd NPs, time-course data in the presence of Pd NPs, O_2 and buffer effect on nanocatalytic 4-NO-1-N reduction, chronocoulograms corresponding to signal and background levels, optimal concentrations of 4-NO-1-N, H_3N-BH_3 and Pd NP−IgG conjugate, nanocatalytic 4-NO-1-N reduction using Au NP, and effect of nonspecific binding on BSA (PDF).

■ AUTHOR INFORMATION

Corresponding Author

*E-mail: hyang@pusan.ac.kr. Fax: (+82)-51-516-7421.

ORCID

Kwangyeol Lee: 0000-0003-0575-7216

Haesik Yang: 0000-0001-7450-5915

Notes

The authors declare no competing financial interest.

■ ACKNOWLEDGMENTS

This research was supported by the National Research Foundation of Korea (2015R1A2A2A01002695, 2017M3A7B4041973, and 2016M3A7B4910538). This research is also supported by the Ministry of Trade, Industry and Energy (MOTIE, Korea) under Industrial Technology Innovation Program (No. 10062995).

■ REFERENCES

(1) Wei, H.; Wang, E. *Chem. Soc. Rev.* **2013**, *42*, 6060−6093.
(2) Nasir, M.; Nawaz, M. H.; Latif, U.; Yaqub, M.; Hayat, A.; Rahim, A. *Microchim. Acta* **2017**, *184*, 323−342.
(3) Lin, Y.; Ren, J.; Qu, X. *Adv. Mater.* **2014**, *26*, 4200−4217.
(4) Kuah, E.; Toh, S.; Yee, J.; Ma, Q.; Gao, Z. *Chem. - Eur. J.* **2016**, *22*, 8404−8430.
(5) Gupta, S.; Huda, S.; Kilpatrick, P. K.; Velev, O. D. *Anal. Chem.* **2007**, *79*, 3810−3820.
(6) Xu, C.; Qu, X. *NPG Asia Mater.* **2014**, *6*, e90.
(7) Gao, L.; Zhuang, J.; Nie, L.; Zhang, J.; Zhang, Y.; Gu, N.; Wang, T.; Feng, J.; Yang, D.; Perrett, S.; Yan, X. *Nat. Nanotechnol.* **2007**, *2*, 577−583.
(8) Das, J.; Aziz, M. A.; Yang, H. *J. Am. Chem. Soc.* **2006**, *128*, 16022−16023.
(9) Nam, J.-M.; Thaxton, C. S.; Mirkin, C. A. *Science* **2003**, *301*, 1884−1886.
(10) Hervés, P.; Pérez-Lorenzo, M.; Liz-Marzán, L. M.; Dzubiella, J.; Lu, Y.; Ballauff, M. *Chem. Soc. Rev.* **2012**, *41*, 5577−5587.
(11) Aditya, T.; Palb, A.; Pal, T. *Chem. Commun.* **2015**, *51*, 9410−9431.
(12) Arruda, T. M.; Shyam, B.; Ziegelbauer, J. M.; Mukerjee, S.; Ramaker, D. E. *J. Phys. Chem. C* **2008**, *112*, 18087−18097.
(13) Retnamma, R.; Novais, A. Q.; Rangel, C. M.; Yu, L.; Matthews, M. A. *Int. J. Hydrogen Energy* **2014**, *39*, 6567−6576.
(14) Mei, Y.; Lu, Y.; Polzer, F.; Ballauff, M.; Drechsler, M. *Chem. Mater.* **2007**, *19*, 1062−1069.
(15) Blaser, H.-U. *Science* **2006**, *313*, 312−313.
(16) Staubitz, A.; Robertson, A. P. M.; Manners, I. *Chem. Rev.* **2010**, *110*, 4079−4124.
(17) Zhan, W.-W.; Zhu, Q.-L.; Xu, Q. *ACS Catal.* **2016**, *6*, 6892−6905.
(18) Wang, X.; Liu, D.; Song, S.; Zhang, H. *J. Am. Chem. Soc.* **2013**, *135*, 15864−15872.
(19) Yang, H. *Curr. Opin. Chem. Biol.* **2012**, *16*, 422−428.
(20) Das, J.; Jo, K.; Lee, J. W.; Yang, H. *Anal. Chem.* **2007**, *79*, 2790−2796.
(21) Dutta, G.; Park, S.; Singh, A.; Seo, J.; Kim, S.; Yang, H. *Anal. Chem.* **2015**, *87*, 3574−3578.
(22) Kang, C.; Kang, J.; Lee, N.-S.; Yoon, Y. H.; Yang, H. *Anal. Chem.* **2017**, *89*, 7974−7980.
(23) Fang, C. S.; Oh, K. H.; Oh, A.; Lee, K.; Park, S.; Kim, S.; Park, J. K.; Yang, H. *Chem. Commun.* **2016**, *52*, 5884−5887.
(24) Potts, J. T. *J. Endocrinol.* **2005**, *187*, 311−325.
(25) Cusano, N. E.; Bilezikian, J. P. *JAMA Diagnostic Test Interpretation* **2014**, *312*, 2680−2681.
(26) Akanda, M. R.; Joung, H.-A.; Tamilavan, V.; Park, S.; Kim, S.; Hyun, M. H.; Kim, M. G.; Yang, H. *Analyst* **2014**, *139*, 1420−1425.
(27) Park, S.; Yang, H. *Analyst* **2014**, *139*, 4051−4055.
(28) Aziz, M. A.; Patra, S.; Yang, H. *Chem. Commun.* **2008**, 4607−4609.
(29) Bard, A. J.; Faulkner, L. R. *Electrochemical Methods: Principles and Applications*, 2nd ed.; John Wiley & Sons: New York, 2001; pp 501−503.
(30) Sharma, L.; Kalia, R. *J. Chem. Eng. Data* **1977**, *22*, 39−41.
(31) Chen, L.; Gorski, W. *Anal. Chem.* **2001**, *73*, 2862−2868.
(32) Ogino, Y.; Takagi, K.; Kano, K.; Ikeda, T. *J. Electroanal. Chem.* **1995**, *396*, 517−524.

DOI: 10.1021/acs.analchem.7b03364
Anal. Chem. XXXX, XXX, XXX−XXX